Thin-Walled Structures 166 (2021) 108074

Contents lists available at ScienceDirect

Thin-Walled Structures

journal homepage: www.elsevier.com/locate/tws

Full length article

Numerical investigation of polyurea coated aluminum plates under hydrodynamic shocks

O. Rijensky *, D. Rittel

Faculty of Mechanical Engineering, Technion- Israel Institute of Technology, 32000 Haifa, Israel

ARTICLE INFO

Keywords:
Polyurea
Protective coating
Hydrodynamic shock
Finite element analysis
Fluid–structure interaction

ABSTRACT

We present a numerical investigation of polyurea (Pu) coated aluminum plates loaded by a hydrodynamic shock wave. This numerical investigation is a follow-up for two previous sets of experiments studying the mechanical behavior of polyurea coated aluminum plates. The aim of the numerical investigations is to add additional insights for designers using polyurea coatings, regarding the importance and relevance of the coated side with respect to the shock intensity, that are not reachable by experimental means only. It appears that the sole consideration of the coated side provides an incomplete picture, whereas the nature of Pu–aluminum *interface* has an influential effect on the overall performance of the coated plate. To comprehend the importance of the interface between the structure (aluminum) and the coating (polyurea), we examine by means of finite element simulations two extreme cases: one in which the layers are not attached at all and one in which the two layers are fully bonded without separation option. Those interfacial conditions are examined for the case of Pu coating on both sides of the aluminum plate with respect to the water. This paper emphasizes the importance of the interface between the aluminum plate and the Pu to achieve optimal survivability of the compound plate against hydrodynamic shockwaves.

1. Introduction

Marine structures are quite vulnerable to threats of various nature, as even a small hull breach can have catastrophic consequences such as the drowning of the structure, be it is an oil rig or a fast-sailing boat. This also applies to the defense context in which ships are exposed to potential explosions (bombs, mines etc.), or to civil targets like oil rigs which are extremely lucrative targets for terror attacks, as their destruction has severe financial and environmental consequences. Another common threat to the structure is the phenomenon known as "wave slamming", i.e. collisions between hull plates of planing boats and the waves resulting in violent shocks.

Consequently, the urge to develop affordable and effective means of protection against hydrodynamic shocks is quite clear. Polyurea coating is a very promising direction of research in an attempt to develop such protective means. It is relatively cheap, simple to apply as a coating on metals, and has a very good resilience in harsh environments.

The use of polyurea as a protective coating is not an entirely new idea. Though polyurea has been in use as an anti-corrosion and abrasion coating from the end of the 80's, it is only in 2000 that the potential of polyurea as a protective coating was uncovered with the work of Knox et al. [1] on retrofitting concrete structures with polymer coating as a protection form blast induced fragmentation. This work exposed the potential of polyurea as an efficient protective layer. In 2006, efforts were directed at optimizing the use of polyurea coatings to improve structural survivability against various dynamic loads by understanding the mechanisms which mitigate shock waves and strengthen the material at high strain rates. Among the first works revealing and utilizing the unique characterizes of polyurea were those of Amirkhizi et al. [2] who presented a numerical model to describe the various thermo-mechanical characteristics of polyurea. Other groundbreaking works are due of Roland et al.[3], Sarva et al. [4], and Yi et al. [5], who presented experimental investigations of polyurea under uniaxial tension and compression at various strain rates. These works outlined the unique viscoelastic features of the material, resulting in a wealth of research works aimed at optimizing polyurea manufacturing and implementing it into new forms of armor.

On the mechanics of materials side, one should mention the results of Grujicic et al. [6] showing the energy absorption capabilities of polyurea form a micromechanical standpoint. This paper presents a meticulous investigation of the material behavior, starting at the unique hard fibers in a soft matrix structure of the block co-polymer, while explaining how the glassy transition of the material mitigates shock waves traveling through it. Other results of the same group that are relevant to the present work are the numerical investigations of the material behavior by molecular dynamics [7,8]. These works reveal

* Corresponding author.
E-mail address: orenrijensky@campus.technion.ac.il (O. Rijensky).

https://doi.org/10.1016/j.tws.2021.108074
Received 23 November 2020; Received in revised form 31 May 2021; Accepted 9 June 2021
Available online xxxx
0263-8231/

List of symbols and abbreviations

Pu	Polyurea
DIC	Digital image correlation
T_g	Glass transition temperature
c_0	Bulk wave velocity
s	Slope of the shock Hugoniot line in the u_s – u_p (up — particle velocity, and us — shock velocity).
Γ	Gruneisen parameter
e	Internal energy in a material
P	Pressure
$K_{(T)}$	Modified bulk modulus
K_0	Reference bulk modulus
J	Jacobian of the deformation gradient tensor
m	Linear correction function to the bulk modulus per the current material temperature.
$G_{(t)}$	Shear modulus at time t
G_∞	Relaxed shear modulus
n	Number of exponentials describing the relaxation
q_i	Relaxation times
p_i	Relaxation times contribution to the shear modulus.
$a_{(T)}$	Time temperature shift
$\mathbf{D}'$	Deviatoric part of the deformation rate tensor.
A, B	Empirical material constants.
C_{TP}	Pressure–temperature equivalence factor.

more on the shock mitigation mechanisms of shock waves traveling through the polyurea medium.

As the present investigation comprises numerical simulations (finite element), it is relevant to list a few attempts made to devise a material model for polyurea which can be incorporated into available FEA packages. First and foremost, comes the above mentioned work of Amirkhizi et al. [2]. This phenomenological model was built following the master curve by Knauss [9], and it was used by numerous researchers as it is relatively simple, accurate and includes many of the salient phenomena of polyurea under dynamic loading conditions. The model will be described in detail in the materials section of this work, as it was the model we used for the Pu's mechanical behavior.

Another important constitutive model for polyurea is due to Shim et al. [10]. This model describes the polyurea's viscoelastic nature using two parallel Maxwell elements. One of the Maxwell elements describes the soft rubbery response of polyurea under low strain rates while the second Maxwell element is used to capture the viscoelastic behavior of the material at high strain rates. This model is not extensively implemented in numerical models, but understanding this relatively simple model (only eight parameters) provides important insights and some intuition regarding the behavior of the material under various conditions. Finally, the results of Li and Lua [11] showing how the inclusion of an Ogden model to describe the hyperelastic behavior of the material, together with a viscoelastic material model, can explain the unique nonlinear characteristics of polyurea.

Some researchers recognized the potential of polyurea and tried to apply it into various applications. Grujicic et al. [12] showed the potential of polyurea in reducing the risk of traumatic brain injury (TBI) when employed as a combat helmet padding, shielding the wearer from blast induced shock waves which are only mildly mitigated by standard helmet paddings. Roland et al. [13] used polyurea laminates to increase the penetration resistance of armor steel plates impacted by high speed projectile. This was achieved by making sure the test temperature was close enough to the polymer's T_g to induce a glassy transition during impact. Raman et al. [14] used polyurea coating to reinforce concrete panels to increase their survivability against an explosion. They performed numerical simulations to show how a polyurea laminated concrete panel deflects less in response to the shockwave created by a TNT charge detonated in air. Hakmon et al. [15] used polyurea as a safety layer to prevent hull breach on thinner than standard planning boat hull plates, as a protection from wave slamming.

Different experimental setups were used to measure the response of polyurea coated plates to underwater shocks. Amini et al. [16,17] measured and simulated the response of polyurea coated steel plates with emphasis on both the coated side as well as the thickness of the coating. Li et al. [18] performed an experimental investigation of polyurea coated 6061 aluminum plates with respect to the coated side and the coating thickness. Rijensky et al. [19] measured the response of polyurea coated aluminum plates to repeated mild shocks mimicking wave slamming. LeBlanc et al. [20] measured the response of polyurea coated composite plates to underwater explosive loadings with emphasis on optimal coating side and coating thickness. These works, together with our works on the matter [19,21], all come to a confusing conclusion. Even if the behavior of aluminum composites and steel plates are not exactly the same, one would nevertheless assume that a similar law applies to all cases, and that the optimal side for application of polyurea coating would be the same for all the above works. Unfortunately, that this is not the case. Some works [18,19] find that it is best to apply polyurea on the loaded side (subsequently referred to wet Pu) of the plate, while others [16,20] find that the coating lies on the opposite side to the load (subsequently referred to as dry Pu). The present numerical investigation is aimed at solving these differences or, at least, shedding some light as to their origin. For that purpose, a numerical model of a typical experimental setup is reported. This model is aimed at reproducing the trends observed in [21], and providing insights regarding the optimal side for lamination application.

The issue of the dynamic interfacial strength of the primer applied between the plate and the coating is seldom considered, at least quantitatively, in such applications. Therefore, we will bond the effect of the interfacial strength by assuming two extreme cases, namely no bonding and perfect bonding. The numerical simulations presented in the sequel do not replicate accurately any specific experiment, but they are aimed at clarifying the role of the interface in the composite plate's deflection along with a better understanding of what is really measured when surface deflections are assessed.

2. Methods

2.1. Problem statement

The simulations presented here are aimed at mimicking generically a typical experimental setup described in detail in [21]. Briefly stated, a specimen plate is confined at the end of a cylindrical anvil filled with water. The other end of the anvil is obstructed by a piston whose back side is in contact with a long steel bar. A compressed air gun accelerates a projectile to hit the far (from piston) side of the bar. A shock wave arises in the bar due to the projectile impact. This shock wave travels through the bar and hits the piston which, in turn, compresses and shocks the water confined within the cylinder. The shockwave travels through the water to load the specimen plate and deform it. A high-speed camera, triggered by the shock wave passing a strain gauge cemented on the incident bar, captures the deformation process. In such experiments, superficial information, such as plate deflection and strains, is recorded and processed using Digital Image Correlation techniques.

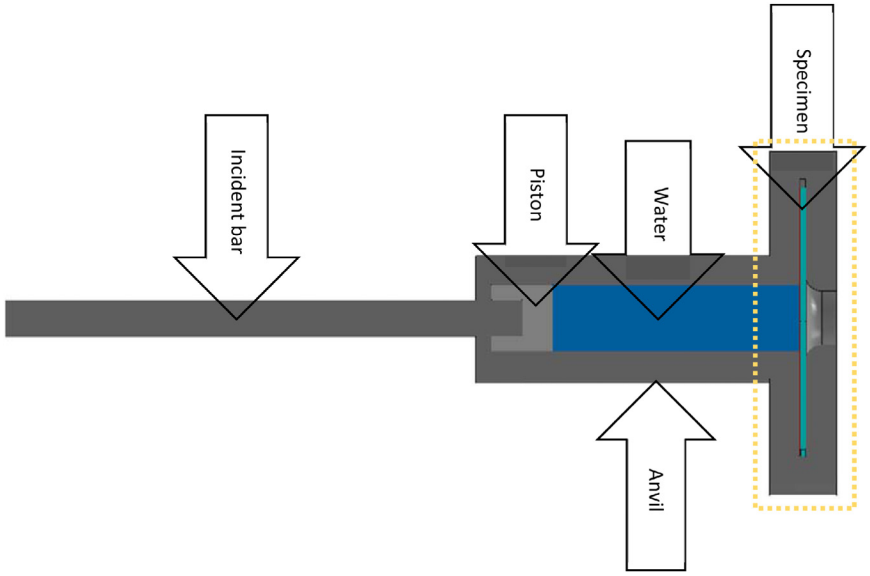

Fig. 1. Section view of the model components.

2.2. Algorithms

The problem at hand consists of simulating the transient response of an aluminum plate coated with polyurea to a pressure wave traveling through water. The first point to notice is that this is a highly transient problem which is best addressed by an explicit time step integration scheme. In this work, we used the commercially available Abaqus-Explicit commercial finite element code [22]. The problem involves both fluids (water) and solids (aluminum, polyurea, and other experimental setup elements), and this requires the choice of a proper fluid–structure interaction simulation method. Since the water is not expected to flow extensively and acts essentially as a shock wave transmission medium, it is not mandatory to divide the problem into two domains (fluid and solid) and solve each domain with a dedicated solver, since the emphasis is on the solid medium. Some methods for such problems include a relatively simple fluid motion into a structural simulation. We experimented with some of these techniques (Eulerian–Lagrangian scheme, acoustic media) to model the fluid–structure interaction, and eventually opted for the Smoothed Particle Hydrodynamics (SPH) [23] method, both for its numerical stability as well as for the ability of Abaqus to use this method together with parallel computing, something that cannot be achieved when solving a Eulerian–Lagrangian problem. This method proved to be very stable even under intense shocks which caused other methods to diverge.

The SPH method is a meshless method in which a material is represented by freely moving particles instead of a permanent grid (mesh). This is a very natural description for fluid flow. The method is very stable and since there is no mesh, there are no computational problem with large deformations or motions. The interaction between the fluid and the structural domains requires no special treatment and is handled by Abaqus' general contact formulation. The general contact algorithm was used defined by "hard" pressure-overclosure normal behavior and penalty tangential behavior with 0.2 friction coefficient, as a stabilizing factor. The normal pressure-overclosure option prevents materials from undergoing mutual penetration by applying a force on contacting nodes. There is no upper bound to the exerted force required to prevent penetration. The tangential behavior "penalty" method states that a frictional force is exerted on surfaces in contact to resist their slippage. The magnitude of this force is calculated as ordinary kinetic friction with respect to the determined coefficient of friction. Friction here is assumed for numerical convenience rather than physical reality.

2.3. Model geometry (solid parts)

The model geometry was designed to mimic the experimental setup described in Rijensky et al. [21]. The different parts partaking in the model are described in Fig. 1 and its detailed view, Fig. 2.

The setup is comprised of a 1.5 m long, 25.4 mm diameter maraging steel incident bar that is in contact with a steel piston. The piston has an indentation with same diameter as the incident bar. Its outer diameter is 46 mm, just like the diameter of the cylindrical cavity of the anvil that holds all the parts together. The cylindrical cavity is filled with water confined between the above-mentioned piston and the specimen plate. The specimen plate is held within a 4.3 mm wide round slit in the pressure cylinder, which is also the overall thickness of the coated plate. All these parts are visible in the cross-sectional view of the simulation shown in Fig. 1. A circular opening in the anvil of 18.65 mm diameter is machined opposite to the water side to allow for plate bulging as can be seen at the top of Fig. 2.

The sharp corner created by this opening was smoothed with a fillet of radius 10 mm to avoid early local shear failure because of local stress concentrations. This fillet changes the boundary condition, causing the edge of the deforming area to be simply supported instead of clamped.

The specimen plate is a 180 mm diameter disk built from two layers, a 0.8 mm thick aluminum layer and 3.5 mm thick polyurea layer. Two configurations of this plate were used in the simulations: In the first, the Pu layer is in contact with the water (subsequently referred to as wet Pu), and in the second (shown in Fig. 2), the aluminum layer is in contact with the water (subsequently referred to as dry Pu).

Two extreme interfacial conditions were considered. For the attached plates, the two layers (Pu and Al) were bound with a tie constraint that keeps both layers moving together, and for that constraint, the aluminum layer was chosen as the master surface and the Pu layer was the slave surface due to the apparent difference in their rigidity (neglecting the viscoelastic nature of polyurea). The separated plates required no special treatment to the interface as the contact algorithm was defined to allow separation of the two independent layers.

The only boundary condition applied to the model is a velocity condition on the far edge of the incident bar defined by the trapezoidal functions shown in Fig. 3. These functions differ from one another by the maximal values of the velocity that they reach. A projectile hitting an incident bar in experiments, enforces a velocity boundary condition which is half of the projectile velocity on the incident bar boundary.

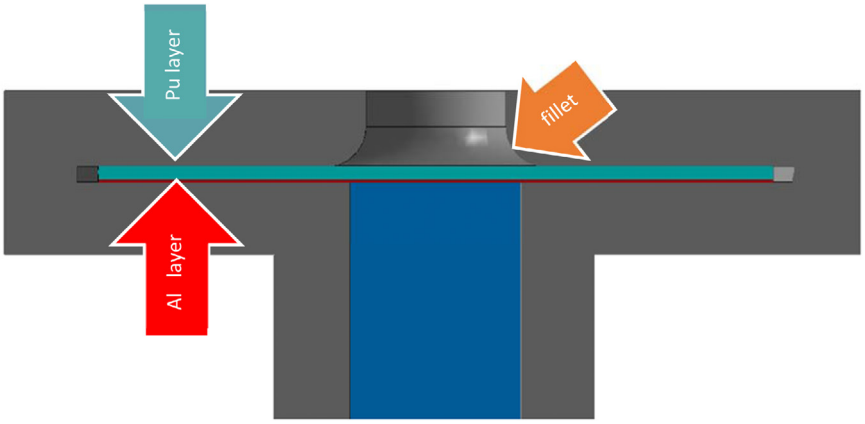

Fig. 2. Detailed view of the region marked with a yellow square in Fig. 1.

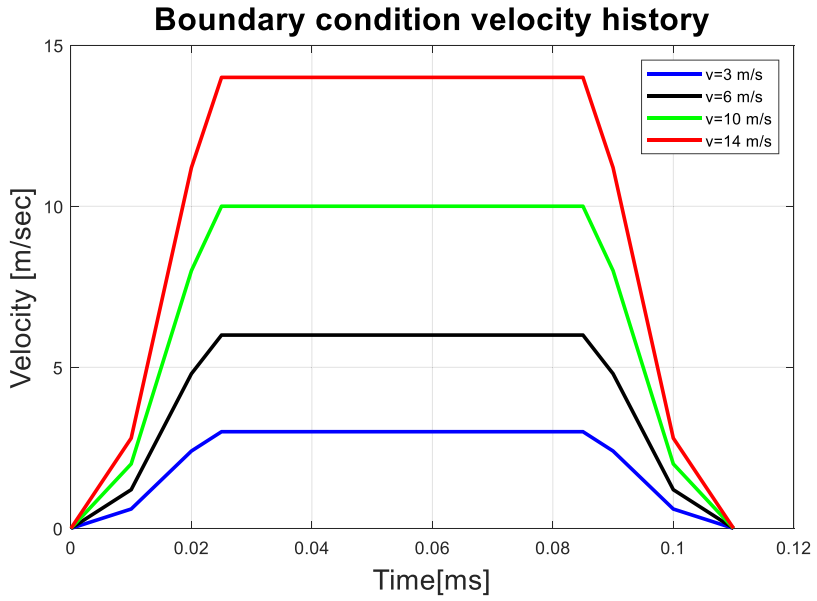

Fig. 3. Velocity boundary conditions trapezoidal pulses.

2.4. Mesh

All parts of the solid model (besides the water) were meshed with C3D8R. This element type is an eight-node cubic element with one integration point at its center making it computationally efficient. All parts were coarsely meshed to reduce calculation times with the exception on the specimen plates and the water where greater detail was needed (see Fig. 4).

The specimen plates were meshed with five layers of elements through the thickness in the thin aluminum layer and seven elements through the thickness it the thicker polyurea layer. The elements size in the other directions was chosen to create reasonably shaped element that are not too thin throughout the thickness. The meshing of the plate is shown in Close-up view of the meshed aluminum layer.

The water was meshed with the same elements but those were converted to particles with a time criterion set to zero (on the first calculation increment), making the type of chosen elements irrelevant as the mesh was only used to set the initial location of the different nodes (particles). The initial distance between the particles was set approximately to 0.2 mm.

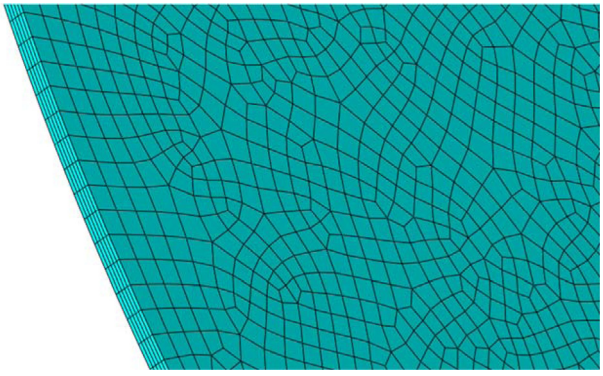

Fig. 4. Close-up view of the meshed aluminum layer.

Table 1
Parameters of the Johnson–Cook model for the aluminum plate [24].

Density Kg/m^3	Young's modulus (GPa)	Poisson's ratio	A (MPa)	B(MPa)	n	m
2660	68.9	0.29	324	114	0.42	1.34

Table 2
The constitutive parameters used in the numerical model for polyurea.

T_{ref} [K]	A	B [K]	C_{tp} [K GPa^{-1}]	C_V [J mm^{-3}K^{-1}]	CTE [K^{-1}]	m [GPa K^{-1}]	n	k_{ref} [GPa]	G_∞ [GPa]
273	−10	107.54	7.2	1.977×10^{-3}	2×10^{-4}	−0.015	4	4.948	0.0224
p_1	p_2	p_3	p_4	q_1 [ms]	q_2 [ms]	q_3 [ms]	q_4 [ms]		
0.8458	1.686	3.594	4.342	463.4	0.06407	1.163×10^{-4}	7.321×10^{-7}		

3. Material models

3.1. Steel

The anvil, incident bar and piston which were made of steel in [21] were modeled using linear elastic material model with parameters matching those of a typical maraging steel. Young's modulus was set to 185 GPa with Poisson's ratio of 0.29. The density of the material was 8000 Kg/m^3. Throughout the experiments, the steel parts remained elastic.

3.2. Aluminum

Aluminum for modeling the specimen plates' base layer was modeled as an elastic–plastic material. Since the aluminum is not the focus of this work, we did not calibrate any analytical model to capture its plastic behavior, and instead used published Johnson–Cook parameters form [24] . The material parameters used to model the elastic–plastic behavior of aluminum in the simulations are summarized in Table 1

3.3. Water

The water was modeled using the first order Mie–Gruneisen equation of state as implemented in Abaqus:

$$P = \frac{\rho_0 c_0{}^2 \eta}{(1-s\eta)^2}\left(1-\frac{\Gamma\eta}{2}\right)+\Gamma\rho_0 e \tag{1}$$

$$\eta = 1-\frac{\rho_0}{\rho} \tag{2}$$

where P is the pressure, c_0 is the bulk wave velocity in the material and s is the slope of the shock Hugoniot line in the u_s-u_p (up — particle velocity, and us — shock velocity). Γ is the Gruneisen parameter and e is the internal energy of the material (which is considered zero by default in Abaqus, that assumption being correct for materials in their reference state). This constitutive equation sets a relation between the density and the pressure of the material. It ignores shear stresses which should otherwise be dealt with independently (these are negligible in fluids) and provides a relatively simple and intuitive model to describe the water undergoing shocks. A similar model was used by other researchers for similar simulations [25]. To account for cavitation in the simplest possible way, we introduced a tensile failure criterion set to 1 KPa with no element deletion.

3.4. Polyurea

Polyurea was modeled according to the constitutive law described in [2]. The model was implemented into Abaqus as a Vumat routine. In this model, volumetric and deviatoric stress are dealt with independently.

The volumetric stress (i.e., pressure) P includes a softening effect due to temperature changes:

$$P = -K_{(T)}\frac{\ln J}{J} \tag{3}$$

$$K_{(T)} = K_0 + m\left(T-T_0\right) \tag{4}$$

here P is the pressure $K_{(T)}, K_0$ are the modified and reference bulk moduli, J is the Jacobian of the deformation gradient tensor and m is a linear correction function to the bulk modulus according to the current material temperature.

Polyurea's viscoelastic nature requires that the full history of strains be considered to find the current state of stress. This is computationally impossible as the calculation will grow longer with each time step. According to the technique described in [2], it is possible to overcome this issue by approximating the shear modulus with a series of decaying exponentials which represent different characteristic relaxation times of the material. Each of these exponentials must be defined by both its relative contribution to the material stiffness as well as a decaying time for the exponential function. A calculation of the shear modulus at a specific time without thermal effects is given by:

$$G_{ref(t)} = G_\infty + \left(1+\sum_{i=1}^{n} p_i e^{\frac{-t}{q_i}}\right) \tag{5}$$

where $G_{(t)}$ is the shear modulus at time t, G_∞ is the relaxed shear modulus , n is the number of exponentials describing the relaxation, and q_i and p_i are the relaxation times and their contribution to the shear modulus respectively.

With this shear modulus, the hereditary integral which computes the deviatoric stress takes the form:

$$\boldsymbol{\sigma}'_{(t)} = \int_0^t 2\frac{T}{T_{ref}}G_{ref(t)}\left(\frac{t}{a_{(T_{(\tau)})}}\right)\mathbf{D}'_{(\tau)}d\tau \tag{6}$$

With $a_{(T)}$ being a time temperature shift function which increases the effect of time on the material when temperature rises, and $\mathbf{D}'$ being the deviatoric part of the deformation rate tensor.

Since temperature changes over time due to dissipation, this integral must be evaluated from $t=0$ at every time step, and this is impossible to do from a computational standpoint.

To allow this integral to be transferred from one step to the next without introducing the concept of a reduced time, a new time scale which changes with temperature and defined as:

$$\xi_{(t)} = \int_0^t \frac{d\tau}{10^{A(T-T_{ref}-P*C_{TP})/(B+T-T_{ref}-P*C_{TP})}} \tag{7}$$

where A, B are empirical constants. This expression was also modified to consider pressure effects on the shear modulus by including C_{TP}, the pressure–temperature equivalence factor and the pressure P. One can see that the pressure and the temperature have reversed effects on the material i.e., temperature rise accelerates the reduced time, so that the material relaxes faster, and pressure has the opposite effect. Introducing the reduced time removes the explicit form of t, $\frac{t}{a_{(T)}}$ in from the hereditary integral making it usable for FEA calculations as follows:

$$\boldsymbol{\sigma}'_{(t)} = \int_0^t 2G_{(t,\tau)}\mathbf{D}'_{(\tau)}d\tau \tag{8}$$

$$G_{(t,\tau)} = \frac{T}{T_{ref}}G_{ref}\left(\xi_{(t)}-\xi_{(\tau)}\right) \tag{9}$$

All the material constants were used exactly as in the original work [2] which formulated this model and are all summarized in Table 2.

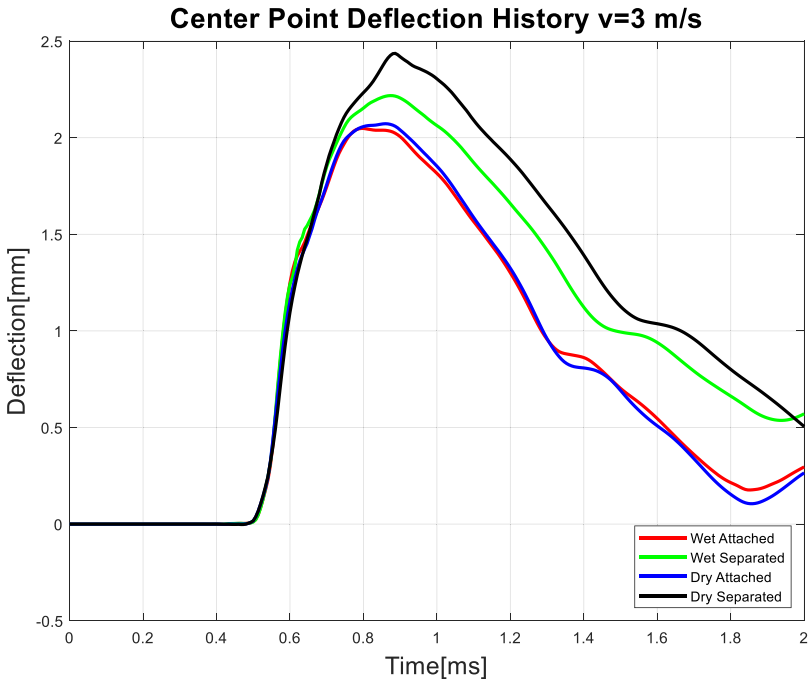

Fig. 5. Center point deflection under velocity boundary condition 3 m/s.. (For interpretation of the references to color in this figure legend, the reader is referred to the web version of this article.)

4. Results

4.1. Center point deflections

The first metric used to assess the plates' performance is their center point deflection. A cube, 5 × 5 mm through the thickness of the aluminum layer was chosen to represent the center point deflection. The mean value of the out of plane (perpendicular to the plate) deflections of all nodes confined within this cube was extracted from the simulations and is presented in Figs. 5 to 8 for each investigated velocity.

Fig. 5 shows that attached polyurea (red & blue) outperforms separated polyurea (black & green), irrespective of the coated side. Dry Pu performs better than wet Pu with the same interfacial condition. During an initial period (of up to *ca.* 0.6 ms), all plates deflect at a similar rate (plot slopes are the same). Past this period, each plate performs differently. Aluminum layer with a separated interface cannot transfer momentum efficiently to the polyurea layer which has good shock mitigation capabilities, leading to more energy being converted into plastic strain as evidenced by larger deflections. It is important to note that this simulation is almost purely elastic in that the accumulated plastic deformation is almost negligible.

Fig. 6 shows again that attached Pu (red and blue) outperforms separated Pu (black and green). As before, dry Pu performs better than wet Pu when considering either only the attached Pu plates or only the separated plated. One can notice that the gap between these two groups narrows, thus reducing the advantage of attached polyurea. Past the initial shock phase, all plates keep deforming at a comparable rate. All in all, one can notice that attached plates mitigate the shock more efficiently than separated plates, and therefore accumulate less plastic strain.

Considering now an impact velocity of 10 m/s (Fig. 7), a clear difference is noticeable with respect to the previous two plots. First, the best performance is achieved by attached Pu on the dry side (blue). Other plates preform very similarly. Both Wet Pu plates' responses are similar, and this is probably due to the fact that the shock pushes the Pu layer against the aluminum layer as shown in the sequel. The separated dry plate (black) shows a marginally worst performance of all tested configurations. Even though the dry attached plate deflected similarly to all the others during initial loading, it bounced back more to achieve the best performance again, showing that the attached Pu layer mitigates the shock.

Fig. 8 shows the center point deflection for a 14 m/s boundary condition velocity. Once again, dry Pu plate outperforms all others. We can see here that separated wet Pu plate outperforms the wet attached plate for the first time. This shows that unique interfacial conditions are required for each load amplitude for an optimal performance. Separated dry Pu plate exhibits the worst shock mitigation as evidenced from its maximal deflection.

Next, a validation of the model will be presented based on the center point responses of different plates to the shock.

4.2. Validation of the numerical results

Throughout this work, we modeled extreme interfacial conditions and their consequences on various aspects of the coated plate deflection. In such simulations, we attempted to replicate the experimental conditions exposed in [21], without exactly modeling every component of the experimental setup, while preserving its salient characteristics. Whereas the experiments were reported for different projectile launching pressures, the current simulations considered projectile impact velocity. Consequently, a one-to-one quantitative comparison is beyond current reach. However, the simulations can be validated qualitatively by comparing experimental and numerical trends. Here, one must keep in mind that whereas the experiments considered only side aspects of the coating, simulations also considered the state of interfacial bonding. Therefore, while a preliminary validating comparison is presented below, one should also consider the additional information conveyed by the simulations about the interfacial bonding condition.

Table 3 below compares 3 experimental [21] and 3 numerical simulations results, where the pressures/impact velocities range from low to medium and high. The table ranks the overall performance of the coated plate. From this table, one can see that the experimentally reported trends are faithfully replicated qualitatively in terms of plate deflection. Let us note again that the interfacial condition is missing from the experiments, however, some conclusions can be inferred from

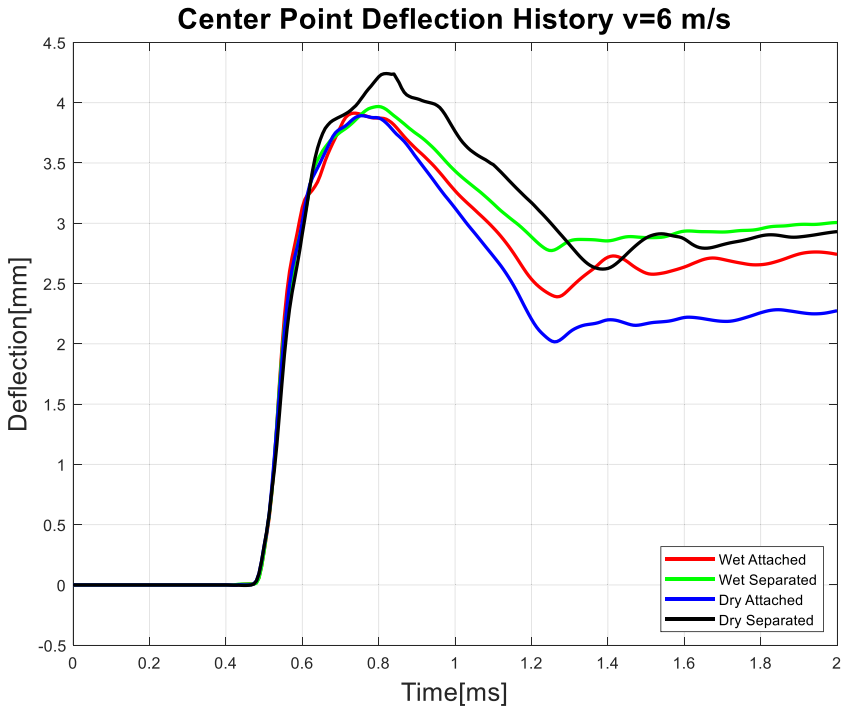

Fig. 6. Center point deflection under velocity boundary condition 6 m/s.. (For interpretation of the references to color in this figure legend, the reader is referred to the web version of this article.)

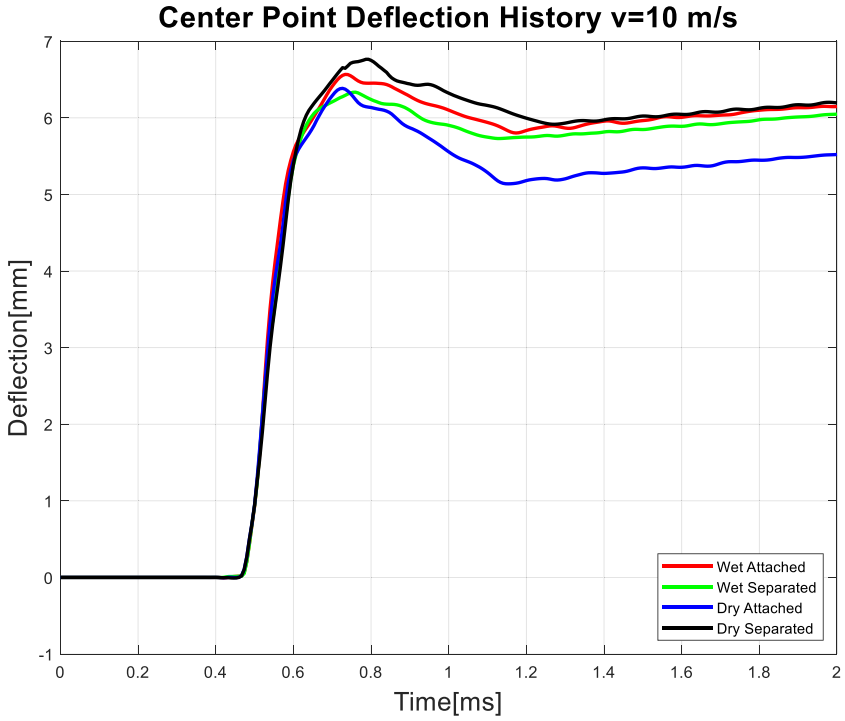

Fig. 7. Center point deflection under velocity boundary condition 10 m/s.. (For interpretation of the references to color in this figure legend, the reader is referred to the web version of this article.)

the match between the measurements and the simulations. More specifically, the numerical simulations, when compared to the experimental results, can assist in the determination of the interfacial state, noting that the latter may eventually evolve from initially attached to detached at some stage.

All in all, the comparisons presented in Table 3 validate qualitatively the numerical simulations, and consequently they validate the main conclusions of this work.

To better understand the interaction between the layers and its' effect on overall plate performance, we next look at the interfacial kinetics between the center points of the two layers.

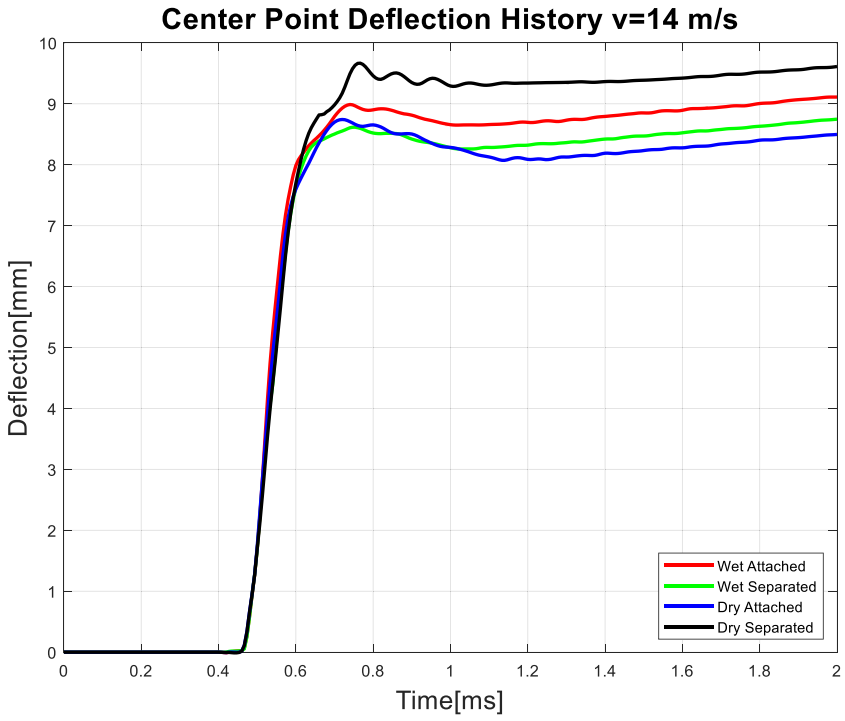

Fig. 8. Center point deflection under velocity boundary condition 14 m/s. (For interpretation of the references to color in this figure legend, the reader is referred to the web version of this article.)

Table 3
Comparison of numerical simulation with experimental outcomes.

Experimental figure [21]	Approx. center point deflection (first shock)	**Conclusion**	Numerical simulations figure	Approx. center point deflection	**Conclusion**
5	1–4 mm	wet pu performs better than dry pu	5	2.5 mm	wet pu **attached** performs better than dry **separated** pu
6	2–5 mm	wet pu performs better than dry pu	6	4 mm	wet pu **attached** performs better than dry **separated** pu
7	6 mm	wet pu = dry pu	7	6 mm	wet pu **attached** = dry pu **separated**

4.3. Interfacial kinetics

The different interface conditions between the layers affect their ability to transfer momentum between the various components of the composite plate. This section investigates the interlayers kinetics during shock loading of the plates, considering only the separated interfacial state. The same area, previously used to calculate the center point deflection, was considered here. The next plots will show the distance between this square at the interface on the aluminum layer and the adjacent square in the polyurea layer. Results are shown in Fig. 9.

The top graph in Fig. 9, shows a small early gap opening in all plates at about 0.5 ms. This effect can be assumed to result from the different wave velocities in the aluminum (typically 6400 m/s) and the Pu (typically 1800 m/s according to the results by Qiao et al. [26]). The shock wave propagating through the steel anvil precedes the shock propagating in the water and reaches the edge of the plate creating a wave moving from the edge of the plate towards its center. Since this wave travels through the polyurea layer and the aluminum layer independently (as the layers are separated) it reaches the center of the aluminum layer first and starts its deflection before the polyurea starts deflecting. This is a relatively weak shock, and the aluminum layer bounces back to meet the polyurea layer before the major shock wave propagating through the water reaches the plate. When this shock hits the plate, the gap is closed and remains closed until the shock has decayed (e.g., 1.5 ms for 3 m/s in wet separated case Fig. 9). Then, the wet separated plate exhibits a gap which grows monotonically. The aluminum layer accumulates plastic strain and remains therefore curved once the shock has passed. Pu, on the other hand, bounces back to its pre-shock shape. This is the origin of this gap. It has no significance to the plates' performance, and it can only be used as an indicator of the end of the shock. This gap can also be seen in Fig. 10 which portrays a central section of the plate at various instants of the deformation.

Considering again the bottom graph in Fig. 9, one can note that a gap opens when separated Pu is placed on the dry side the previous early gap. This separation happens during the deformation of the plate (0.45–1.2 ms). The meaning is simple and yet very important. During deformation, the Pu is not in contact with the aluminum. If there is no contact, the aluminum layer is left unprotected from the shock as it cannot transfer momentum and energy to the Pu layer, rendering the Pu redundant. As the projectile velocity grows (and with it, the shock intensity), this gap between layers opens for a shorter duration. i.e., in weak shock, dry Pu is almost ineffective, and as the shock intensifies, it becomes more effective. This gap can also be seen in Fig. 11 which shows the plate 's centerline at selected instants of the deformation.

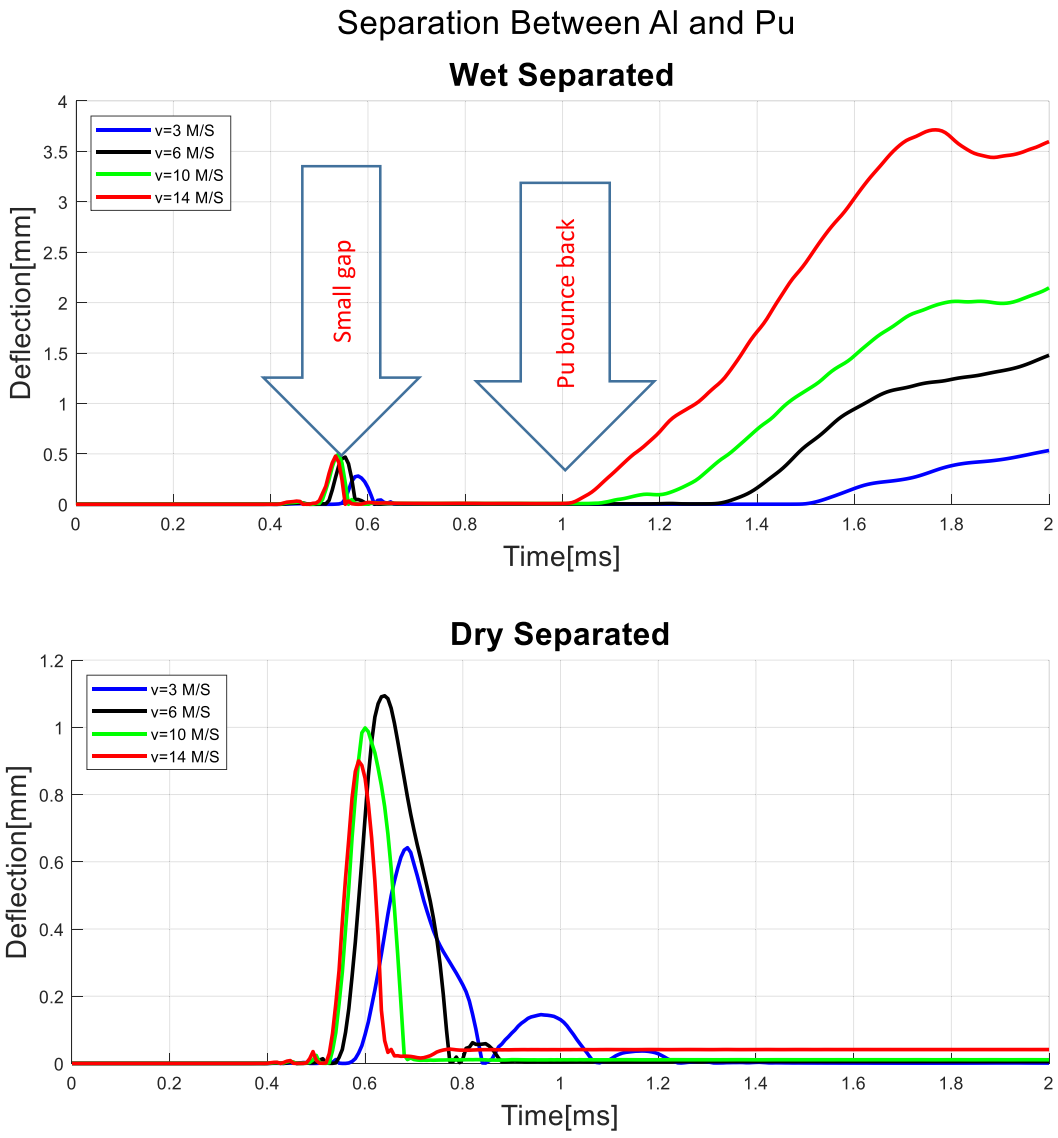

Fig. 9. Interlayer separation for various impact velocities. (For interpretation of the references to color in this figure legend, the reader is referred to the web version of this article.)

4.4. Polyurea deflection reduction

To better understand the effectiveness of the polyurea coating, we simulated the response of bare aluminum plates to the same loading conditions. We extracted the center point deflections of these simulations and calculated the polyurea deflection reduction as the difference between the center point deflection of a coated aluminum plate and the center point deflection of a bare aluminum plate. This metric is aimed at showing the efficiency of the coating. The lower the value, the more performant the coating (as more deflection had been reduced). Table 4 presents the final values of the deflection reduction in millimeters at the end of the simulation.

As it seems, Pu on the dry side with strong adhesion performs best under all loading conditions. On the other hand, the separated wet Pu plate shows the worst performance on mild impacts with the separated dry Pu plate showing similar outcomes. On stronger shocks, the separated dry Pu plate, shows again the worst performance. Considering the interlayer separation, this is not surprising at all as the gap leaves the aluminum layer in the dry separated case unprotected throughout most of the shock, i.e., bare aluminum.

One should also consider the wet Pu results as for some engineering applications, dry Pu is generally not an option. When comparing the two different interlayer constraints in the wet Pu configuration, one

Table 4
Polyurea coating effective deflection reduction in millimeters — final values. The best performance for every projectile velocity is marked in green and the worst is marked in red.

Specimen Plate type / Projectile velocity	Wet Pu - attached	Wet Pu - separated	Dry Pu - attached	Dry Pu - separated
3 m/sec	-1.82	-1.57	-1.85	-1.61
6 m/sec	-2.31	-2.05	-2.75	-2.13
10 m/sec	-2.31	-2.41	-2.94	-2.26
14 m/sec	-3.91	-4.28	-4.53	-3.41

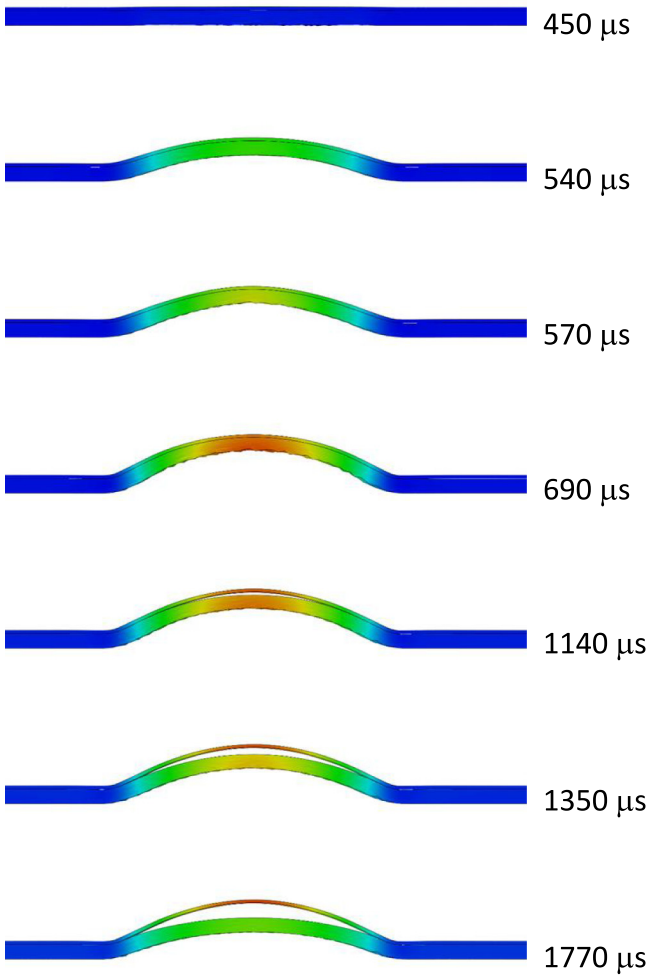

Fig. 10. Diametral cross-section of the wet Pu separated plate at various instants throughout the shock. from top to bottom at:t=450 μs, t = 540 μs, t = 570 μs, t = 690 μs, t = 1140 μs, t = 1350 μs and t = 1770 μs.

can see that attached plate shows better or same performance under mild shocks while separated plate performs better under strong shocks.

4.5. Center line Von-Mises stress distribution

The next plots (Fig. 12) show the Von-Mises strain distributions at the final step of the simulation, long after the plate stopped deforming and reached its final shape. Stresses were extracted from a center line at the interface between the aluminum layer and the polyurea layer.

Looking at the shape of the distribution for a 3 m/s projectile velocity (top left plot), one can see that dry plates (black and blue) accumulate the stress at their center versus wet plates (green and red) which have two stress lobes on the sides of the plate. The separated dry Pu plate reach lower stress level and has a more evenly spread, thus desirable, distribution. As the projectile velocity increases, all the plates tend to reach a similar stress distribution, culminating at 14 m/s, namely two large side lobes and a low center stress. This corresponds well with the failure as captured by experiments in [19,21]. One also can see that the dry attached plate undergoes lower or equal stresses compared with other plates for all experiments, and less pronounced side lobes meaning lower stress concentration, a very desirable feature when discussing protection for maritime applications.

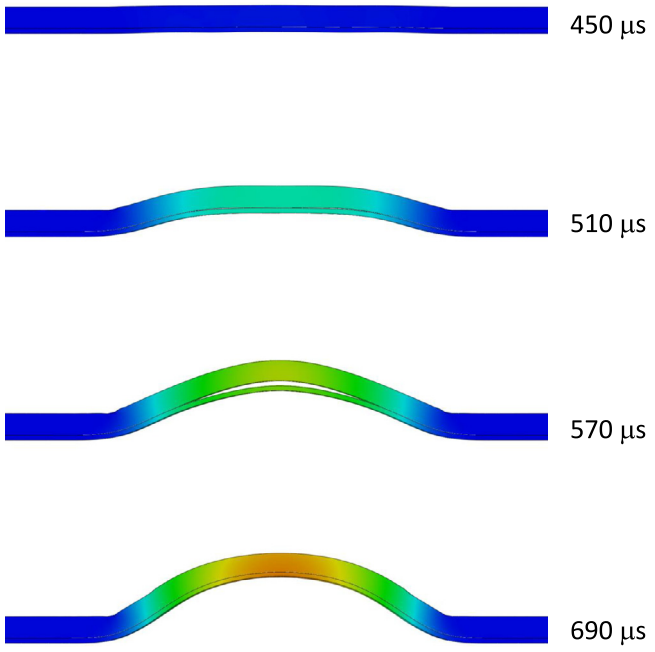

Fig. 11. Diametral cross-section of the dry Pu separated plate at various instants throughout the shock. from top to bottom at:t = 450 μs, t = 510 μs, t = 570 μs and t = 690 μs.

4.6. A short remark on surface measurements using 3D-DIC for bulge tests

Many researchers use surface measurement techniques (e.g., 3D-DIC - digital image correlation) to measure the deformation field in bulge tests. The choice is clear as DIC is a reliable, well established method that does not affect the experiment (contactless). DIC is relatively simple to employ, requires only standard equipment and produces the full field of strains with great accuracy. In this section, we will review the simulation results as if they were measured by a 3D DIC system. As DIC can only measure the outermost surface facing the cameras we will extract the center point deflection of the plate based on 5 mm X 5 mm square around the center of the plate at the outer surface, whether this surface is aluminum (wet Pu specimens) or polyurea (dry Pu specimens).

Fig. 13 shows a comparison between actual (volumetric averaged) center point deflections and deflections as determined by a 3D DIC system for projectile velocities of 10 m/s (left — top and bottom) and 14 m/s (right — top and bottom). It is readily noticed that the comparable plots are not the same. 3D-DIC obtained result tend to underestimate the deflection of dry plates. For example, under 10 m/s load, dry attached plate (blue line) reached 5.5 mm deflection when considering the volume averaged result vs. 5 mm deflection when "using" 3D DIC, namely a 10% difference in measurement. This discrepancy in measurement might lead the designer to think that the dry attached plate performs much better than other plates (1 mm difference in deflection is 20% better), when in fact, the margin is not as big as the DIC measures. This happens because DIC is based on images in which the polyurea layer is visible. The measurement of the plate deflection is in fact a measure of the coating's deflection, which can lead to incorrect analysis of the results and related conclusions. This effect is most clearly seen from the behavior of the dry separated plate (black line), on which one can see the violent fluctuations of the flexible coating which are much weaker when considering the volumetric averaged result. This means that the use of DIC (and other similar measurement techniques measuring the back surface of the specimen plate) requires an appropriate FEA simulation or other validation technique before the outcomes and firm conclusions can be drawn for such problems. In

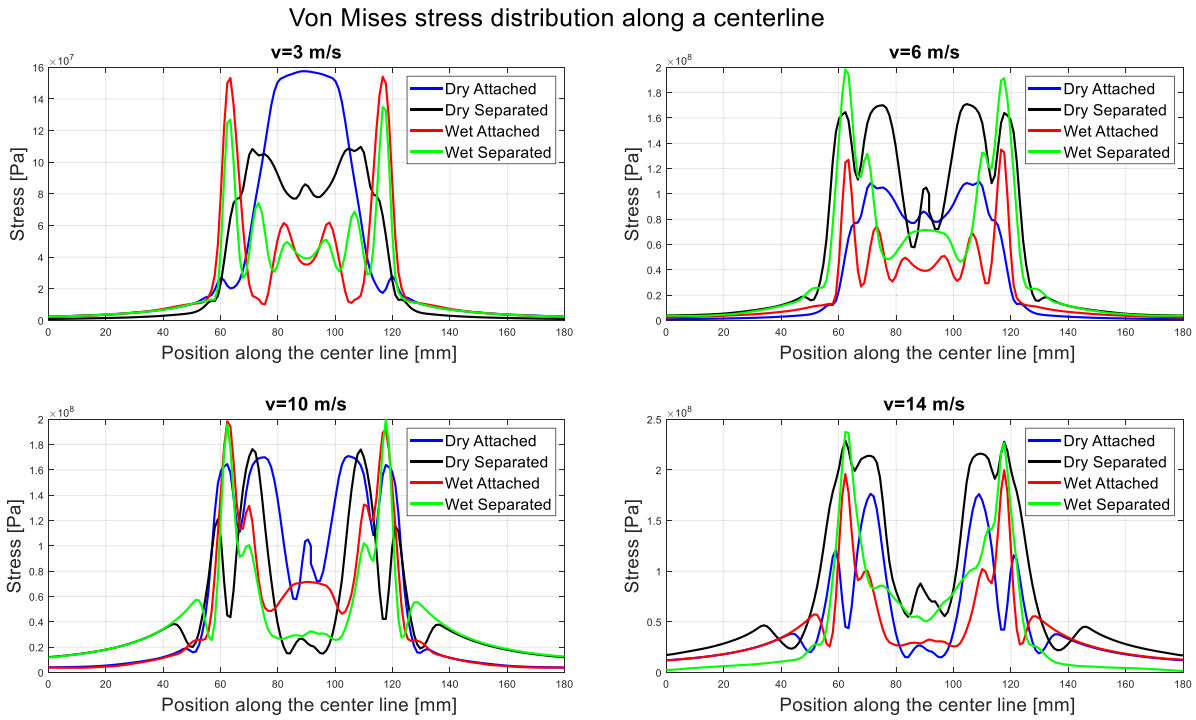

Fig. 12. Von-Mises strain distribution past the deformation at various velocity boundary conditions. From top left and moving clockwise: v = 3 m/s, v = 6 m/s, v = 10 m/s, v = 14 m/s.. (For interpretation of the references to color in this figure legend, the reader is referred to the web version of this article.)

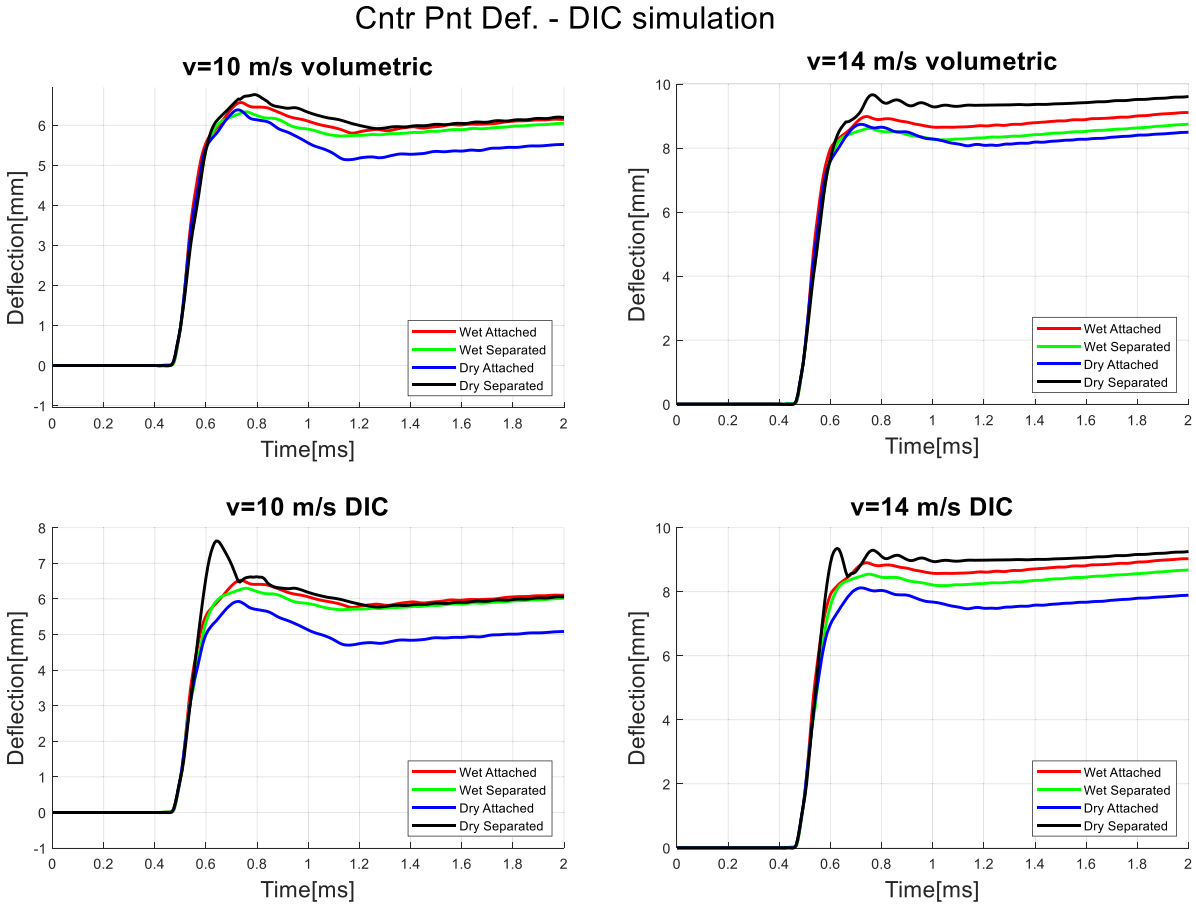

Fig. 13. Comparison between volumetric averaged center point deflection and center point deflections as those would have been captured by a 3D DIC system.. (For interpretation of the references to color in this figure legend, the reader is referred to the web version of this article.)

other words, the interfacial condition, discussed all along this work, affects the reliability of the measurements.

5. Conclusions

We have presented and validated numerical simulations results following a set of experiments aiming to shed light on the importance of the coated side. The simulation revealed that together with the polyurea coated side, one should also consider the strength characteristics of the primer used before this coating.

We have shown that the interlayer interface can change the performance of the coated plate from best to worst. When considering the results presented here, it is clear that a strong adhesive and a coating applied to the dry side (attached dry Pu) can yield the best performance. Simulations suggest that dry attached Pu configuration allows polyurea to absorb energy more efficiently and mitigate the shock wave with less energy converted to aluminum plastic strain. On the other hand, our past experiments [19,21] in which the exact dynamic interfacial strength was not measured, but definitely involved bonding, have shown that wet Pu can prevent cavitation induced damage which can be a leading mechanism to failure of a plate.

It has also been shown that deflections measured 3D-DIC may contain some inaccuracy when the interface gets detached. Improving the experimental accuracy of the measured deflections of the aluminum plate requires complementary numerical simulations.

CRediT authorship contribution statement

O. Rijensky: Conceptualization, Methodology, Formal analysis, Investigation, Writing - original draft, Writing - review & editing, Visualization. **D. Rittel:** Writing - review & editing, Supervision, Funding acquisition.

Declaration of competing interest

The authors declare that they have no known competing financial interests or personal relationships that could have appeared to influence the work reported in this paper.

References

[1] K.J. Knox, P.E. Michael, I. Hammons, P.E. Timothy, T. Lewis, J.R. Porter, Polymer materials for structural retrofit.

[2] A.V. Amirkhizi, J. Isaacs, J. McGee, S. Nemat-Nasser, An experimentally-based viscoelastic constitutive model for polyurea, including pressure and temperature effects, Philos. Mag. 86 (2006) 5847–5866, http://dx.doi.org/10.1080/14786430600833198.

[3] C.M. Roland, J.N. Twigg, Y. Vu, P.H. Mott, High strain rate mechanical behavior of polyurea, Polymer (Guildf) 48 (2007) 574–578, http://dx.doi.org/10.1016/j.polymer.2006.11.051.

[4] S.S. Sarva, S. Deschanel, M.C. Boyce, W. Chen, Stress–strain behavior of a polyurea and a polyurethane from low to high strain rates, Polymer (Guildf) 48 (2007) 2208–2213, http://dx.doi.org/10.1016/j.polymer.2007.02.058.

[5] J. Yi, M.C. Boyce, G.F. Lee, E. Balizer, Large deformation rate-dependent stress–strain behavior of polyurea and polyurethanes, Polymer (Guildf) 47 (2006) 319–329, http://dx.doi.org/10.1016/j.polymer.2005.10.107.

[6] M. Grujicic, B. Pandurangan, T. He, B.A. Cheeseman, C.-F. Yen, C.L. Randow, Computational investigation of impact energy absorption capability of polyurea coatings via deformation-induced glass transition, Mater. Sci. Eng. A 527 (2010) 7741–7751, http://dx.doi.org/10.1016/j.msea.2010.08.042.

[7] M. Grujicic, R. Yavari, J.S. Snipes, S. Ramaswami, J. Runt, J. Tarter, et al., Molecular-level computational investigation of shock-wave mitigation capability of polyurea, J. Mater. Sci. 47 (2012) 8197–8215, http://dx.doi.org/10.1007/s10853-012-6716-4.

[8] M. Grujicic, B. Pandurangan, W.C. Bell, B.A. Cheeseman, C.-F. Yen, CL. Randow, Molecular-level simulations of shock generation and propagation in polyurea, Mater. Sci. Eng. A 528 (2011) 3799–3808, http://dx.doi.org/10.1016/j.msea.2011.01.081.

[9] W.G. Knauss, Viscoelastic material characterization relative to constitutive and failure response of an elastomer, 2004.

[10] J. Shim, D. Mohr, Rate dependent finite strain constitutive model of polyurea, Int. J. Plast. 27 (2011) 868–886, http://dx.doi.org/10.1016/j.ijplas.2010.10.001.

[11] C. Li, J. Lua, A hyper-viscoelastic constitutive model for polyurea, Mater. Lett. 63 (2009) 877–880, http://dx.doi.org/10.1016/j.matlet.2009.01.055.

[12] M. Grujicic, W.C. Bell, B. Pandurangan, T. He, Blast-wave impact-mitigation capability of polyurea when used as helmet suspension-pad material, Mater. Des. 31 (2010) 4050–4065, http://dx.doi.org/10.1016/j.matdes.2010.05.002.

[13] C.M. Roland, D. Fragiadakis, R.M. Gamache, Elastomer–steel laminate armor, Compos. Struct. 92 (2010) 1059–1064, http://dx.doi.org/10.1016/j.compstruct.2009.09.057.

[14] S.N. Raman, T. Ngo, P. Mendis, T. Pham, Elastomeric polymers for retrofitting of reinforced concrete structures against the explosive effects of blast, Adv. Mater. Sci. Eng. 2012 (2012) 1–8, http://dx.doi.org/10.1155/2012/754142.

[15] R. Hakmon, N. Drimer, Verifying a new hydro-elastic design method for planing boats by full-scale sea trials, Ships Offshore Struct. (2020) 1–15, http://dx.doi.org/10.1080/17445302.2020.1781327.

[16] M.R. Amini, J. Isaacs, S. Nemat-Nasser, Investigation of effect of polyurea on response of steel plates to impulsive loads in direct pressure-pulse experiments, Mech. Mater. 42 (2010) 628–639, http://dx.doi.org/10.1016/j.mechmat.2009.09.008.

[17] M.R. Amini, J. Simon, S. Nemat-Nasser, J. Isaacs, S. Nemat-Nasser, Investigation of effect of polyurea on response of steel plates to impulsive loads in direct pressure-pulse experiments, Mech. Mater. 42 (2010) 615–627, http://dx.doi.org/10.1016/j.mechmat.2009.09.009.

[18] Y. Li, Z. Chen, T. Zhao, X. Cao, Y. Jiang, D. Xiao, et al., An experimental study on dynamic response of polyurea coated metal plates under intense underwater impulsive loading, Int. J. Impact Eng. 133 (2019) 103361.

[19] O. Rijensky, D. Rittel, Polyurea coated aluminum plates under hydrodynamic loading: Does side matter? Int. J. Impact Eng. 98 (2016) 1–12, http://dx.doi.org/10.1016/j.ijimpeng.2016.07.006.

[20] J. LeBlanc, A. Shukla, Response of polyurea-coated flat composite plates to underwater explosive loading, J. Compos. Mater. 49 (2015) 965–980, http://dx.doi.org/10.1177/0021998314528263.

[21] O. Rijensky, D. Rittel, Experimental investigation of polyurea coated aluminum plates under strong hydrodynamic shocks, Thin-Walled Struct. 154 (2020) 106833, http://dx.doi.org/10.1016/j.tws.2020.106833.

[22] U. Abaqus, Abaqus2006.

[23] J.J. Monaghan, Smoothed particle hydrodynamics, Annu. Rev. Astron. Astrophys. 30 (1992) 543–574.

[24] D.R. Lesuer, G.J. Kay, M.M. Leblanc, Modeling large-strain, high-rate deformation in metals, 2001.

[25] H.D. Espinosa, S. Lee, N. Moldovan, A novel fluid structure interaction experiment to investigate deformation of structural elements subjected to impulsive loading, Exp. Mech. 46 (2006) 805–824, http://dx.doi.org/10.1007/s11340-006-0296-7.

[26] J. Qiao, A.V. Amirkhizi, K. Schaaf, S. Nemat-Nasser, G. Wu, Dynamic mechanical and ultrasonic properties of polyurea, Mech. Mater. 43 (2011) 598–607, http://dx.doi.org/10.1016/j.mechmat.2011.06.012.